HONO Emissions from Western U.S. Wildfires Provide Dominant Radical Source in Fresh Wildfire Smoke

Qiaoyun Peng[1], Brett B. Palm[1], Kira E. Melander[1], Ben H. Lee[1], Samuel R. Hall[2], Kirk Ullmann[2], Teresa Campos[2], Andrew J. Weinheimer[2], Eric C. Apel[2], Rebecca S. Hornbrook[2], Alan J. Hills[2], Denise D. Montzka[2], Frank Flocke[2], Lu Hu[3], Wade Permar[3], Catherine Wielgasz[3], Jakob Lindaas[4], Ilana B. Pollack[4], Emily V. Fischer[4], Timothy H. Bertram[5], Joel A. Thornton[1*]

[1]Department of Atmospheric Sciences, University of Washington, Seattle, WA, USA.
[2]National Center for Atmospheric Research, Atmospheric Chemistry Observations & Modeling Laboratory, Boulder, CO, USA
[3]Department of Chemistry and Biochemistry, University of Montana, Missoula, MT, USA
[4]Department of Atmospheric Science, Colorado State University, Fort Collins, CO, USA
[5]Department of Chemistry, University of Wisconsin, Madison WI, USA

* *Correspondence to*: Joel A. Thornton (joelt@uw.edu)

ABSTRACT: Wildfires are an important source of nitrous acid (HONO), a photo-labile radical precursor, yet *in situ* measurements and quantification of primary HONO emissions from open wildfires have been scarce. We present airborne observations of HONO within wildfire plumes sampled during the Western Wildfire Experiment for Cloud chemistry, Aerosol absorption and Nitrogen (WE-CAN) campaign. HONO to CO enhancement ratios close to the fire locations ranged from $0.7 - 17$ pptv ppbv^{-1}, with the median similar to previous observations of temperate forest fire plumes. Measured HONO to NO_x enhancement ratios were generally factors of 2, or higher, at early plume ages than previously reported. Enhancement ratios scale with modified combustion efficiency and certain nitrogenous trace gases, which may be useful to estimate HONO release when HONO observations are lacking or plumes have photochemical exposures exceeding an hour as emitted HONO is rapidly photolyzed. We find that HONO photolysis is the dominant contributor to hydrogen oxide radicals ($HO_x = OH + HO_2$) in early stage (< 3 hours) wildfire plume evolution. These results highlight the role of HONO as a major component of reactive nitrogen emissions from wildfires and the main driver of initial photochemical oxidation.

KEYWORDS: biomass burning emissions, radical source, wildfire smoke, western United States

1 Introduction

Nitrous acid (HONO) is emitted directly into the atmosphere through various combustion processes, from vehicle exhaust[1] to biomass burning[2]. As a source of both hydroxyl radicals (OH) and nitrogen oxides (NO_x = NO + NO_2), HONO emissions can have a significant impact on the atmosphere's oxidizing capacity[3].

During biomass burning, biomass nitrogen is combusted to form a range of inorganic and organic N containing species, such as HCN, HNCO, HONO, NO, NO_2, N_2O, N_2, etc. The speciation among these various forms at the source remains actively researched[4,5]. In laboratory studies of biomass burning, Veres et al.[6] observed HONO to carbon monoxide (CO) emission ratios between 1.2×10^{-3} and 4.6×10^{-3} mol mol^{-1} depending on the fuel type. Yokelson et al.[7] observed direct emissions of HONO with a study-average emission factor of 0.26 ± 0.13 g kg^{-1} from pasture fires during the Amazon dry season. Stockwell et al.[8] determined the overall HONO to CO emission factor to be 0.10 g kg^{-1} in regional Indonesian peat fires during the FLAME-4 laboratory experiments.

In wildland fire plumes, the fate and importance of HONO is influenced by fuel characteristics (e.g. moisture and N content), combustion conditions, sunlight, smoke plume opacity, cloud cover, and dilution rates[9]. Photolysis is expected to be the dominant daytime loss pathway for HONO with a lifetime of 10-20 minutes at midday and unit quantum yield to OH and NO[10,11]. Previous *in situ* HONO measurements in biomass burning plumes were largely confined to prescribed fires, aged smoke far from the source, or outside of the typical western U.S. fire season[12–14]. While laboratory studies are useful for characterizing the initial conditions of wildfire emissions, they cannot replicate the variable and changing combustion conditions of wildfires, particularly for species as short-lived as HONO. Fuels are typically heterogeneous in composition and burn unevenly, creating variable plume heights and smoke transport at different phases of combustion[15]. Moreover, atmospheric and ecosystem conditions prior to and during fires affect burning conditions and fuel moisture content, which in turn affect emissions.

Uncertainties in HONO primary emissions limit the ability to understand and simulate photochemical production of O_3 and secondary aerosol within wildfire plumes. Several prognostic models of biomass burning plumes have found that inclusion of additional HONO emissions accelerates initial plume chemistry and improves the agreement between simulated and measured O_3 production[16–18]. Thus, more detailed information on primary HONO emissions at the source level is essential for simulating fire-generated HONO and subsequent photochemical impacts.

Herein, we use *in situ* measurements collected from the NCAR/NSF C-130 aircraft during the Western Wildfire Experiment for Cloud chemistry, Aerosol absorption and Nitrogen (WE-CAN) campaign, which was carried out in summer 2018 in the western U.S., to examine HONO and associated trace gases in fresh smoke plumes from large wildfires. Several fire plumes with known source locations and fuel types were sampled in a pseudo-Lagrangian approach, which proved useful for the study of near-source HONO and its impact on subsequent gas-phase photochemistry in plumes with physical ages from less than half an hour to greater than 5 hours for the same fire. Moreover, the number of distinct fires sampled allow us to evaluate potential drivers of variability in HONO emissions.

2. Methods

2.1 WE-CAN campaign overview and instrumentation

The WE-CAN campaign took place from 22 July to 14 September 2018. The research aircraft was based in Boise, ID from 24 July to 31 August 2018, and this period is the focus of our paper. More detail on the campaign can be found in the Supplemental Information (SI). Here we focus on observations collected by the University of Washington (UW) High Resolution Time of Flight Chemical Ionization Mass Spectrometer (HRToF-CIMS). Measurements of other relevant species and parameters by different instruments on board are summarized in Table S1.

The HRToF-CIMS with iodide (I^-) adduct ionization was employed as described in detail previously[19,20], and in the SI, with the main modification being the use of a sheath-flow facilitated, coaxial IMR region[21].

Under laminar flow conditions, only 25% of gases are expected to diffuse to the inlet wall and back to the center of the flow from which we sample into the ion-molecule reaction (IMR) region. Background signals were measured every 60 seconds by overflowing the IMR sampling orifice with UHP N_2 for 6 s as described previously[20,21]. The sampling inlet was also overflowed with UHP N_2 during flight every 20

5 min for 12 s. To prevent titration of reagent ions and thus nonlinear responses in wildfire plumes, the sample flow entering the IMR was diluted as needed with a known flow rate of ultra-high purity (UHP) N_2 to maintain constant reagent ion count rates.

We calibrated the HRToF-CIMS response to HONO, and a range of other trace gases (Table S2) before and after the campaign, and tied the calibration to HCN, Cl_2, and HCOOH standards used to monitor

10 relative changes in instrument sensitivity. We generated HONO following Febo et al. [22], flowing HCl across a $NaNO_2$ salt bed to promote the reaction

$$HCl(g) + NaNO_2(s) \rightarrow NaCl(s) + HONO(g). \qquad (R1)$$
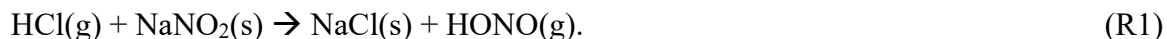
15 HONO output from R1 is variable in time, depending upon humidity and exposure. We therefore simultaneously measured the output utilizing an independently calibrated total reactive nitrogen (NO_y) instrument operating a heated molybdenum catalyst coupled to a chemiluminescence NO analyzer. We also bubbled the output into vials containing a Griess reagent (sulfanilic acid and 2-naphthylamine in dilute acetic acid) which reacts with NO_2^- in solution to form a visible light-absorbing compound. The

20 vials were then analyzed by UV-Vis absorbance at 528 nm as commonly done for aquatic NO_2^-/HONO measurements following Xue et al.[23]. The two calibration approaches resulted in the same HONO calibration factor to within combined uncertainties, of 2.1 ± 0.6 counts per second/pptv HONO/10^6 counts per second of reagent ions, which also agrees well with our independently determined value used for the previous WINTER campaign[20,21]. More details on HONO calibration and interference checks, such as

25 from $H^{13}COOH$ and NO_2 reactions on inlet surfaces, can be found in the SI (Figures S1 and S2).

Maps of WE-CAN research flights are shown colored by the corresponding mixing ratio of HCN (Figure 1) or HONO (Figure S3) measured by the HRToF-CIMS. Altogether 258 fire plumes were sampled across

the16 research flights (RFs). Most flights took off at approximately 14:00 local time ± 1 hour, with a flight duration of approximately 6 hours. More information can be found at https://www.eol.ucar.edu/field_projects/we-can.

Results and discussion

3.1 Primary HONO emissions

In Figure 1, we show the average of HONO and CO concentrations, normalized to their respective maximum mixing ratios, measured during the horizontal transects of 19 fire plumes. For each plume intercept, prior to normalizing by the maximum, we subtracted the respective "background ambient" concentration to determine the plume enhancement, where the median of 20 seconds of ambient abundances just prior to intercepting the plume are used as the background. We have divided the intercepts into "near-field" and "far-field" representing how far downwind from the fire the plume was sampled and thus how long the smoke has been in the atmosphere. The threshold for physical "age" (see SI) of the near-field intercepts is < 40 min, while > 1 hour for those in the far field. The insets show the absolute mixing ratios measured during typical fresh and aged plume intercepts for HONO and CO.

From these plume intercepts, we wish to calculate the normalized excess mixing ratio (NEMR), also called enhancement ratio (EnR), which has been widely adopted to connect smoke plume observations to fire emissions[24,25]. It is defined as

$$\text{NEMR}_X = \Delta X / \Delta Y = (X_{plume} - X_{bkg})/(Y_{plume} - Y_{bkg}) \hspace{3cm} (1)$$

where ΔX and ΔY are the absolute excess concentration of target species X and reference species Y relative to the ambient background, respectively. Reference species Y is used to account for plume dilution by entrainment of background air in the near field, and has most commonly been CO, given its slow chemistry.

5

We evaluated the various choices for determining NEMR, such as the ratio of maximum concentration enhancements in the plume, the ratio of integrals of concentrations across the entire plume[26], and the slope of linear least square fits of ΔX versus ΔY. We chose to use the ratio of maximum concentration enhancements, specifically the ratio of mean of the top 5% of concentrations measured in an intercept, because of the expected short photolytic lifetime of HONO in the atmosphere. As illustrated in Figure 1, HONO plume transects are narrower than CO, and the difference in width becomes more prominent as the plume ages downwind. As the plume ages, it is turbulently diffusing and thus spreading in spatial extent, as indicated by the wider CO transects in the far-field compared to the near-field. HONO transects, in contrast, become if anything narrower in the far-field compared to the near-field, and certainly compared to those of CO. As discussed more fully below, this trend is largely driven by the changing HONO photolysis frequency along the plume transect (Figure S4), and is indicative that HONO emitted by the fire is being lost relative to the emitted CO during transport (as expected).

At the plume edges, mixing of the smoke plume with cleaner background air leads to less aerosol light extinction and thus faster HONO photolysis. In addition, at the top of the plume, photolysis rates are actually enhanced by scattering from the plume below. Not only do these behaviors imply a complex 3-D variation in the chemical processing of fresh wildfire plumes, with both dilution and photochemistry enhanced at the plume edges[27], but they also suggest that using linear fits of $\Delta HONO$ to ΔCO across the plume intercept, plume-average concentrations, or even integrals over the plume intercepts would bias $NEMR_{HONO}$ low. Similarly, low time resolution observations of HONO (e.g. < 1 Hz) would also bias estimates of HONO emission ratios low if the role of edge effects on HONO abundances were not taken into account. Using only the top 5% of 1Hz HONO concentrations within a plume intercept are thus our best attempt to address this bias by focusing more towards the central, optically thicker, part of plumes, but measurements at any point downwind of the fire will be potentially biased by HONO losses.

The emission ratio (ER) is a special case of the NEMR, which is reserved for measurements taken at the source, i.e., in the freshest smoke plumes[28], and is more of a characteristic of fuel type and burning conditions, while NEMR may undergo substantial changes downwind of the source due to differential

6

dilution, chemistry, and deposition. In the following discussions, we report NEMR$_{HONO}$ determined within 1 hour of smoke emissions as approximations to its ER for consistency with previous methods[27], and evaluate factors affecting its variability. Given HONO's short photolytic lifetime, we thus expect our NEMR to be lower limits to the ER.

5

Figure 2 shows HONO to CO NEMR from the emission plume passes for 19 different fires sampled across 10 different flights during WE-CAN. We have also labeled each with a corresponding physical age estimate. As described above, the NEMRs in plumes with estimated physical ages less than 1 hour were assumed to represent the emission ratios for that species, relative to CO or NO$_x$. Ages of plumes clearly

10 affected by more than 1 fire, e.g., as determined by satellite observations and in-flight observations, are considered unknown and excluded from this analysis. NEMRs computed using the entire plume integration method are shown in Figure S5 for comparison, and while broadly similar were consistently lower by an average of 40% for HONO to CO NEMR, and 29% for HONO to NO$_x$ NEMR. Tables S3 and S4 list the quantification methods, ranges and other relevant information for HONO ER in the

15 literature as well as in this study.

As indicated in Figure 2, HONO is present in substantial amounts in the early stages of most plumes, with HONO to CO ER spanning from 0.65 to 17.2 pptv ppbv^{-1} (average 5.3 ± 5.2 pptv ppbv^{-1}). The high HONO ER inferred from some of the youngest plume intercepts highlights the importance of direct fire emissions

20 to HONO abundances, and the overall large variations in HONO ERs suggest differences in meteorological conditions, fuel type, plume reactivity, location and distance from the source[24,29]. Our range of HONO to CO NEMR covers values measured in past laboratory and field studies[6,7,13,30–32] (see shading in Figure 2) that sampled fire emissions across several fuel types in the U.S., where the flaming stage HONO to CO NEMR range was reported as approximately $2 – 5$ pptv ppbv^{-1}. The reported emission

25 factors of HONO and CO in Akagi et al. (2011) imply that HONO to CO NEMRs range from 1.8 to 7.0 ppt·ppb^{-1} in temperate forests, while ranging from 5.9 to 10.7 pptv ppbv^{-1} in tropical forests[13], which are of the same magnitude as the highest HONO to CO NEMR observed during WE-CAN. Neuman et al. (2016) determined that the HONO to CO ratio ranged from 1.3 to 5.2 pptv ppbv^{-1} in flaming stage fires

using airborne measurements over the Southeast U.S. at night[33]. Study-wide HONO NEMRs across different age ranges are shown in Figure S6.

To assess whether fire-to-fire differences in the HONO to CO NEMR are caused by the variable nitrogen content of fuels, it is useful to compare ΔHONO to ΔNO_x, which is also emitted during the flaming phase (Burling et al., 2010). The observed HONO to NO_x ER during WE-CAN ranged from 0.25 to 1.4 pptv pptv^{-1} (average 0.72 ± 0.34 pptv pptv^{-1}), for fires sampled 10 – 33 km downwind (corresponding to 0.3 – 1.0 h transport after emission), as shown in Figure 2. Figure S7 shows scatter plots of HONO to CO and NO_x for the closest plume transect in each fire during the campaign.

Our ΔHONO/ΔNO_x ERs clearly lie above most previous determinations. Trentmann et al. first described significant, direct emissions of HONO at ~0.03 pptv pptv^{-1} of NO_x in a savanna fire[16]. Later, Keene et al.[2] determined ΔHONO/ΔNO_x values ranging from 0.048 to 0.23 pptv pptv^{-1} for different Southern African biomass samples in the laboratory. Yokelson et al.[7] observed ΔHONO/ΔNO_x of ~0.14 pptv pptv^{-1} from Brazilian pasture fires. The laboratory studies by Burling et al.[34] found the fire-integrated molar emission ratios of HONO relative to NO_x ranged from approximately 0.03 to 0.20 pptv pptv^{-1}, with higher values observed for southeastern fuels, while later airborne measurements from prescribed burning in southwestern U.S. by Burling et al.[30] revealed systematically higher ΔHONO/ΔNO_x molar ratios spanning from 0.077 to 0.22 pptv pptv^{-1}. Stockwell et al.[8] reported the ΔHONO/ΔNO_x ratio was ~0.13 pptv pptv^{-1} in cooking fires through a series of laboratory measurements. Selimovic et al.[35] detected a HONO to NO_x NEMR of 0.9 pptv pptv^{-1} from an Engelmann spruce canopy fire burned in the FIREX Fire Lab experiments, while reporting a study average ΔHONO/ΔNO_x of 0.21 ± 0.13 from various fuel types, suggesting fresh, moister conifer-canopy fuels may drive higher HONO to NO_x NEMR.

The collective range of ~0.03 – 0.9 pptv pptv^{-1} in the HONO to NO_x NEMRs assembled from these prior studies implies high fire-to-fire variability in HONO emissions, not just from burning conditions, but also from fuel type and fuel characteristics such as moisture and nitrogen content[2,9,34]. Additional factors that can affect reported HONO to NO_x and HONO to CO NEMRs include HONO photochemistry after

emission and measurement artifacts. Previous field measurements were mostly carried out in well-mixed plumes that had photolysis conditions close to clear sky. The large differences compared to previous measurements may reflect WE-CAN's overall higher sampling frequency closer to fire sources, where the more rapid post-emission loss of HONO compared to NO_x, as illustrated by the differences between Figure S2b and S2c, is less significant. The relative change of HONO to NO_x following emission is smaller than the corresponding change in HONO to CO over the same timescale, given that CO remains constant aside from dilution, while NO_x and HONO both dilute and react, so these photochemical effects are not necessarily able to explain all the differences in the HONO to NO_x NEMRs. It is not clear to what extent past measurements of NO_x were contaminated by HONO (or vice versa). For example, NO_x is often measured by catalytic conversion of NO_2 to NO as well as photolytic conversion with wavelengths < 400 nm which will also convert some fraction of HONO to NO, biasing the reported HONO to NO_x NEMR low. The NO_2 measurement made during WE-CAN used photolysis by LED having output optimized to 398 nm, with half power reached at ± 6 nm, implying minimal HONO conversion. The large variability in $\Delta HONO/\Delta NO_x$ within WE-CAN, and the relatively small set of previous observations suggests that previous studies may simply not have sampled fires with the fuel nitrogen content, moisture content, Modified Combustion Efficiency (MCE), etc. of those sampled during WE-CAN. Thus, we conclude that the fuel type and characteristics, as well as fire conditions, are most important in setting the HONO to NO_x emission ratio with large variations from fire to fire and across the fire season.

3.2 HONO evolution and contribution to radical chemistry

During WE-CAN, multiple fires were sampled in a pseudo-Lagrangian fashion, which allowed for investigations into the chemical evolution of the primary emissions downwind from the source. Figure 3 displays the study-wide HONO to CO NEMR evolution in the first few hours of aging, where the points are colored by the average HONO photolysis frequency (j_{HONO}) measured in each plume transect. The median HONO to CO NEMR of this sample population decays by more than 90% in less than 1 hour, which in turn suggests an e-folding time of about 20 minutes. An exponential fit (dashed magenta curve) to this observed decay in $\Delta HONO/\Delta CO$ yields a decay constant of 0.058 min^{-1}(with 95% confidence

9

bounds 0.053 - 0.063), which is nearly identical to the median observed HONO j-value (0.057 min⁻¹). An offset of 0.096 pptv ppbv⁻¹ was included in the fit function so that the curve passes through all the data at higher plume ages. However, the physical meaning of this offset is unclear given that it implies HONO mixing ratios near or below our 1 Hz detection limit (~20 pptv) and so we refrain from interpreting what

5   it implies in terms of potential HONO steady state in aged plumes.

The rapid decay of HONO in Figure 3 is a sign of its impact on chemical processing within the smoke plume and, as noted above, that the emission ratios relative to CO are likely biased low. The youngest plume ages in Figure 3 are ~ 20-30 min transport time from the source, equivalent to 1 to 2 photolysis

10   lifetimes depending on plume *j*-values. Further downwind, where plume ages exceed 2 hours, HONO mixing ratios drop to tens of pptv, which are close to the CIMS detection limit for HONO (Lee et al., 2018) and the ambient background mixing ratios, as shown in Figure S8. Figure 3 suggests the possibility to correct the measured HONO NEMR to account for the HONO lost to photolysis. However, we do not have measurements closer to the source to constrain such an estimate. Given that closer to the fire, plume

15   opacity is likely increasing substantially, and plume vertical motions become more important than the horizontal motions, which we use to estimate plume age, a simple exponential function to estimate HONO at t = 0 may lead to substantial error. Thus, our reported ER for HONO are likely lower limits, and could be larger (e.g., by factors of 2 or more), but by how much remains uncertain..

20   The photolysis of HONO yields OH radicals and NO. In Figure 4, we show that the photolysis of HONO dominates the primary HO$_x$ (OH + HO$_2$) radical production over the first ~1.5 h of atmospheric transport in the wildfire plumes sampled during WE-CAN. We used campaign-wide in-plume observations to generate an observationally constrained estimate of the average primary radical source strength within plumes as a function of plume age:

25

$$P(HO_X) = j_{HONO}[HONO] + 2j_{HCHO}[HCHO] + j_{CH_3CHO}[CH_3CHO] + \emptyset_{OH}j_{O^1D}[O_3] + j_{HNO_3}[HNO_3] +$$
$$\sum_i [O_3](k_i[alkene_i]) \qquad (2)$$

More details are elaborated in the SI. HONO photolysis is the most important single primary source observed in fresh wildfire plumes, with maximum values of approximately 2 pptv s^{-1}. HONO contributes over 70% in plumes with age shorter than an hour, and accounts for approximately 20% of HO$_x$ production even in plumes with physical ages of 3 hours. HCHO photolysis becomes more important than HONO at physical plume ages >1.5 h, but absolute radical production rates drop substantially after the first ~ 1 hours, explaining in part the sustained relative contribution of HONO. O$_3$ photolysis is the third largest contributor overall to the total radical production rate within WE-CAN sampled plumes, but is most important in background air. The large radical source strength in aged (>3 h) fire plumes which is comparable to that of plumes with age ~1 h may stem from the increase in both the mixing ratio of secondary products like O$_3$ and photolysis rates. The dominant role of HONO as the primary radical source, and its relatively rapid decay, suggests that wildfire plumes are highly photochemically active in the first few hours after emission, and then become much less active, closer to background air, thereafter.

3.3 HONO NEMR Variability

In wildfires, a variety of nitrogen containing species are emitted, including NH$_3$, HONO, NO$_x$, and HCN, acetonitrile (CH$_3$CN) and isocyanic acid (HNCO)[6,36]. These nitrogenous gases are emitted to varying degrees depending on fuel and combustion conditions[30,37]. Rarely is it possible to directly measure the fuels consumed at each burning stage, thus we aim to develop an understanding from the WE-CAN campaign of what drives variability from fire to fire in the HONO emission relative to longer-lived trace gases such as CO and HCN.

Setting aside HONO photolysis as perhaps the dominant driver of HONO NEMR variability at any point downwind of a fire, we focus on relationships among various trace gases and combustion conditions measured as close to the fires as possible. HONO mixing ratios in more aged smoke can be quite low due to its fast decay; HONO can also be formed by multiphase processes[38] and thus measurements of plumes with older physical lifetimes may not reflect direct emissions. Therefore, to analyze HONO emission

characteristics, we focus on plume intercepts with physical age shorter than the instantaneous HONO photolysis lifetime to minimize the impact of HONO photolytic loss after emission on our conclusions.

The release of fuel nitrogen and its chemical speciation depends significantly on the heating rate and fuel rank, i.e., the relative amount of nitrogen contained in aromatic structures relative to that in amine structures[39]. At combustion temperatures over 1000 K, increased fuel rank tends to produce more HCN, while decreased fuel rank favors NH_3 formation. These pyrolysis products then undergo further in-flame processing in the flaming stage[40,41]. It is hypothesized that HONO emission results from reaction of OH radicals with fuel derived NO in the vicinity of the flame, where fast oxidation of HCN and NH_3 also occur[42]. Thus, HONO emissions are expected to anti-correlate with HCN and NH_3, as they are intermediate products that are being oxidized in the flame chemistry, while HONO emissions are expected to correlate with MCE and NO_x, corresponding to higher combustion temperatures which favor more oxidized nitrogen. MCE is a proxy for the degree of flaming versus smoldering combustion:

$$MCE = \frac{\Delta CO_2}{\Delta CO_2 + \Delta CO} \qquad\qquad (3)$$

where ΔCO_2 and ΔCO are background-corrected mixing ratio enhancements of CO_2 and CO, respectively[40,43]. MCE ranged from 0.86 to > 0.94 in WE-CAN, suggesting some of the fire to fire variation in our reported ERs results from burning conditions alone. For major wildfires covering large areas, flaming and smoldering may occur concurrently, similar to the condition where many different smaller fires burn at the same time[13]. The co-existence of two combustion phases is common in plumes sampled during WE-CAN, as reflected by a large number of MCEs between flaming and smoldering MCE cutoffs. That said, the effective MCE in an plume intercept explains some of the large variability in the HONO NEMRs (factor of ~10) across the various fires sampled during WE-CAN (Figure 5c). Similarly, $\Delta HONO/\Delta CO$ is negatively correlated with $\Delta NH_3/\Delta CO$ as well as with $(\Delta HCN+\Delta CH_3CN)/\Delta CO$ (Figure 5a and 5b); both these parameters are expected to be larger when flame temperatures are lower and at lower MCEs. Previous work showed that NH_3/NO_x molar ratio was negatively correlated with MCE for a range of fuels, and that the emission factor of NH_3 and HCN are

anti-correlated with MCE[30,44–46]. Others found that NO_x and HONO are positively correlated with MCE[6]. Pyrolysis experiments with a series of biofuel model compounds reveal that the HNCO/HCN ratio is highly dependent on flame temperature while only slightly dependent on the type of compounds[47,48]. The emission of these species as well as the relative partitioning between reduced and oxidized fuel nitrogen appears to depend on both fuel nitrogen content and MCE[30,37], and are therefore potentially a good reference set for evaluating biomass burning conditions.

We define a broader metric, the ratio of reduced N to total N emitted, R_N, which serves as a proxy of fire temperature and oxidizing conditions, with higher values representing higher combustion temperatures and more oxidation.

$$R_N = \frac{HCN + CH_3CN + NH_x}{HCN + CH_3CN + NH_x + HNCO + NO_x + (NO_z - HONO)} \tag{4}$$

NH_x is total (gas+particle) NH_3, and NO_z represents oxidized reactive nitrogen species such as PAN and other organic nitrates, $2*N_2O_5$, and total (gas+particle) nitrate. R_N without HONO in the denominator is highly correlated with our measured HONO enhancements ($R^2 = 0.74$), as shown in Figure 5d. It is likely a more stable metric for estimating HONO emissions when a lack of observations or plume age do not allow direct quantification of HONO release assuming dry deposition is not significant. For example, HONO is often not measured during wildfire smoke studies, or a smoke plume is sampled several hours or more downwind of the source, in which the majority of emitted HONO will have photolyzed. The relationships in Figure 5 provide a means of estimating what the emitted HONO was in such cases and therefore its contribution to the primary radical source during plume evolution.

3.4 Atmospheric Implications

The above results highlight the importance of wildfires as a primary HONO source over the Western U.S. in summer. To our knowledge, our study has reported the highest HONO emission ratios in wildfire plumes. However, our HONO emission ratios are essentially convolutions of the initial emission and any

13

post-emission processes (e.g., photolysis, radical recombination, multiphase chemistry) that may have taken place during plume transport and aging, and are thus potentially lower limits. The focus on fresh biomass burning plumes allowed us to observe how the starting chemistry varies with fuel nitrogen, combustion efficiency, and other trace gas emission, providing an additional constraint on the release of

5 HONO. We show that HONO emissions scale with MCE as well as measures of fire temperature and oxidation conditions, likely reflecting that emissions of this species are driven by flaming combustion with high temperatures.

The HONO NEMRs presented here are likely critical to interpret the evolution of other trace gases and

10 to initiate models intending to represent rapid oxidation within biomass burning plumes. While a complete assessment of plume radical chemistry is beyond the scope of this work, further investigations of the impact of these HONO emissions on downwind chemical evolution with a suite of models is warranted. Moreover, the variation of HONO photolysis frequencies and concentrations between the center and edges of the plumes that we observe suggests that a 3-D chemical plume model is ultimately needed for

15 a complete description of smoke plume chemical evolution and dispersion.

30

FIGURE CAPTIONS

5   **Figure 1.** (left) WE-CAN flight tracks colored and sized by HCN mixing ratios. For symbols with HCN mixing ratios greater than 500 pptv, the color scale stays the same. (right) Binned, averaged, and normalized horizontal plume transects of HONO and CO excess mixing ratios in the near field (upper panel, physical age < 40 min) and far field (lower panel, physical age > 1 h) plumes. The plume cross-sections have been aligned so that their maxima define the plume center (distance = 0). The mean physical

10   age is 28 min for the near-field plumes and 137 min for far field plumes. Shading represents the standard deviations for each bin. The average aircraft speed is ~ 128 m/s. In both cases, HONO plume widths are narrower than those for CO, likely due to the faster photolysis of HONO at the plume edges (see text). The insets show the absolute mixing ratios for example near-field (top) and far-field (bottom) plume transects from RF 3.

15

    Figure 2. HONO enhancement ratios (derived from top 5% integration) relative to CO (top) and NO_x (bottom) in the freshest plume pass for each fire sampled, sorted in descending order of HONO to CO NEMR. The error bars represent the combined instrumental uncertainties summed in quadrature. The top axis shows the respective plume age. Selected reference HONO NEMR ranges from past campaigns

20   are denoted for comparison. Plumes with physical ages greater than 1 h are shown in blank markers.

    Figure 3. Campaign-wide ΔHONO/ΔCO enhancement ratio evolution with plume age colored by HONO photolysis frequency. Box-and-whisker plots (boxes: 25th and 75th percentiles; whiskers: 10th and 90th percentiles; horizontal lines: median) represent 30-minute binned data. The magenta curve is an

25   exponential fit, with constant offset, to the median ΔHONO/ΔCO in each age bin.

    Figure 4. (top) Average relative contribution of different radical sources to HO_x radicals versus plume age of all western wildfire plumes sampled in WE-CAN; (bottom) HO_x production rate of different radical sources versus plume age.

30

    Figure 5. Scatter plots of HONO NEMR versus different tracers: (a) NH_3/CO, (b) $(HCN+CH_3CN)$/CO, (c) MCE, (d) $(HCN+CH_3CN+NH_3)/(HCN+CH_3CN+HNCO+NO_x+NH_3)$, for fresh plumes within HONO photolysis lifetime derived from j(HONO) measurements. Correlation coefficients (R^2) were derived from bivariate linear regressions of all plotted data.
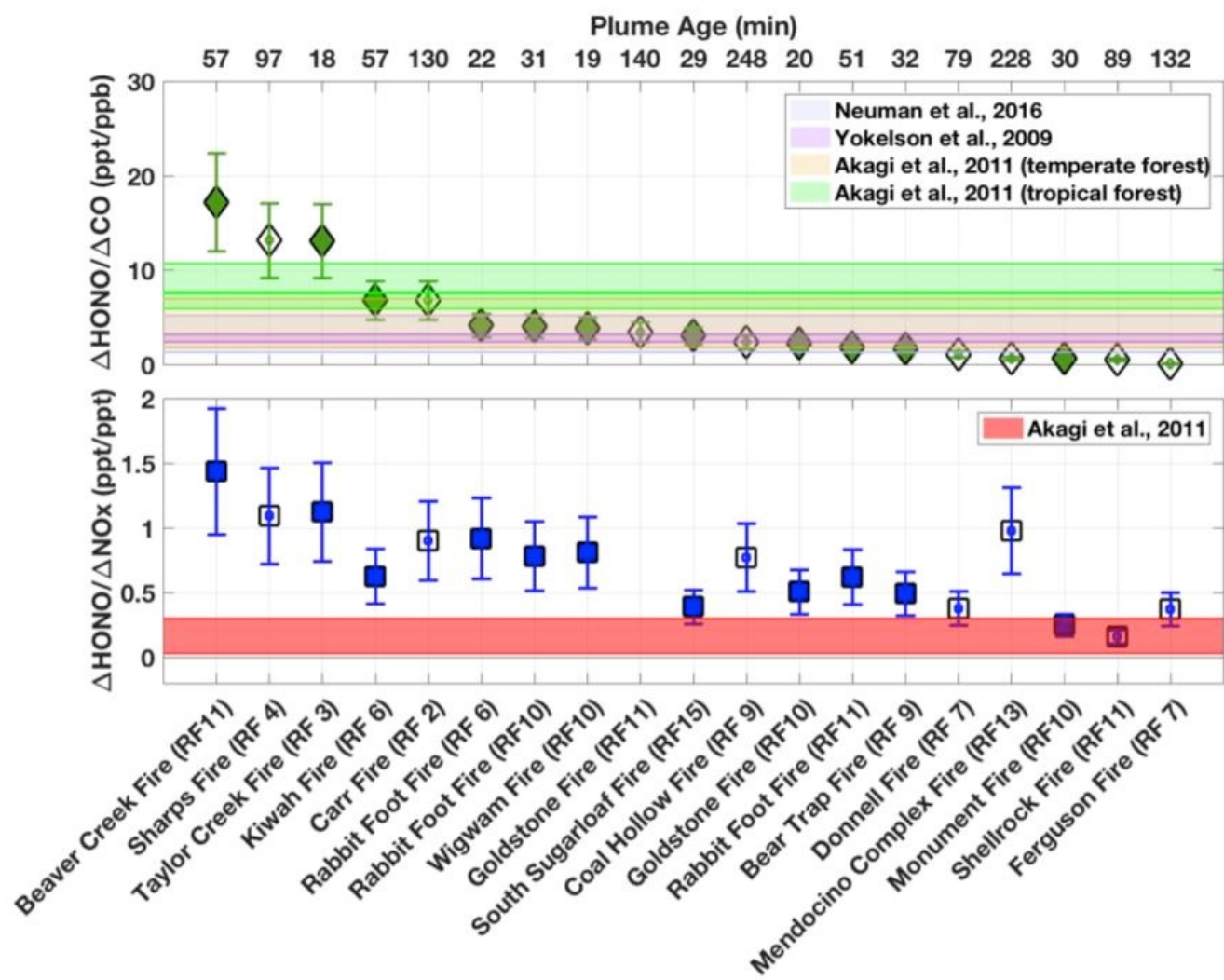
35

Figure 1
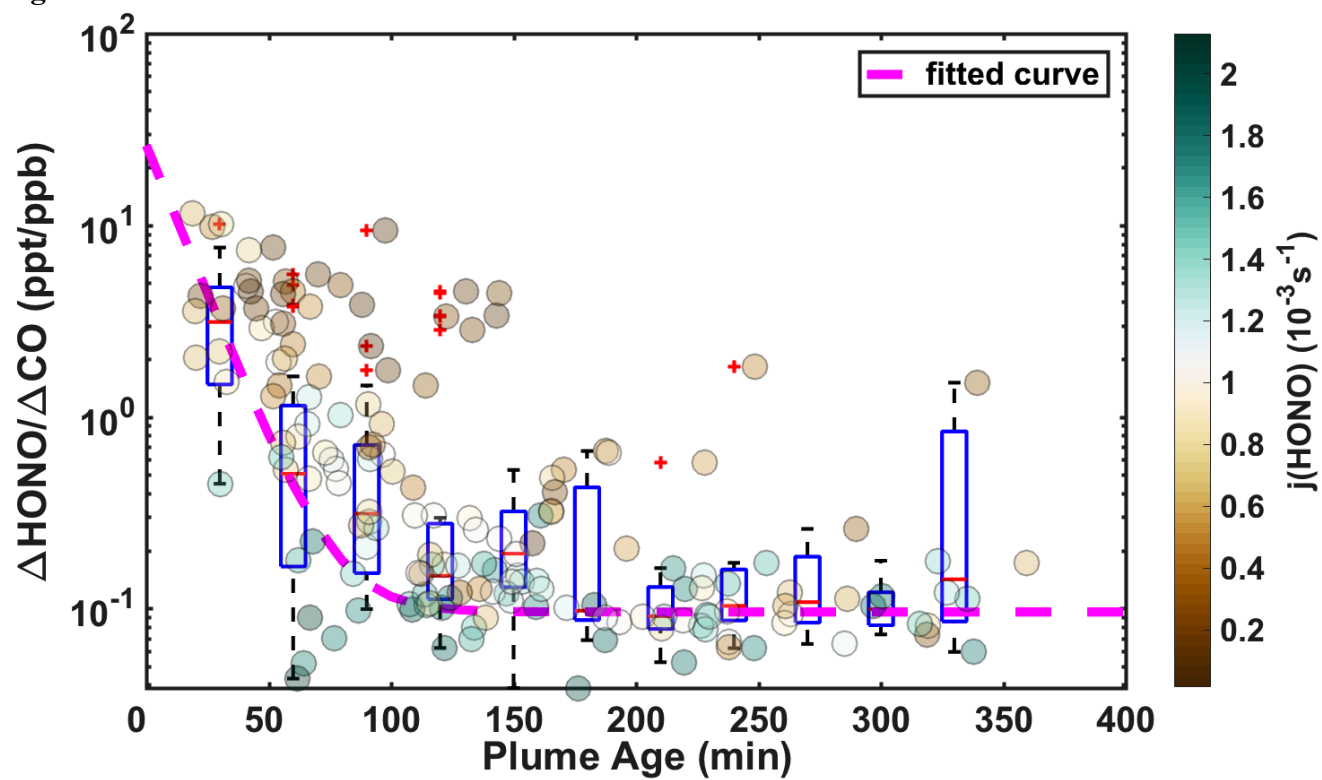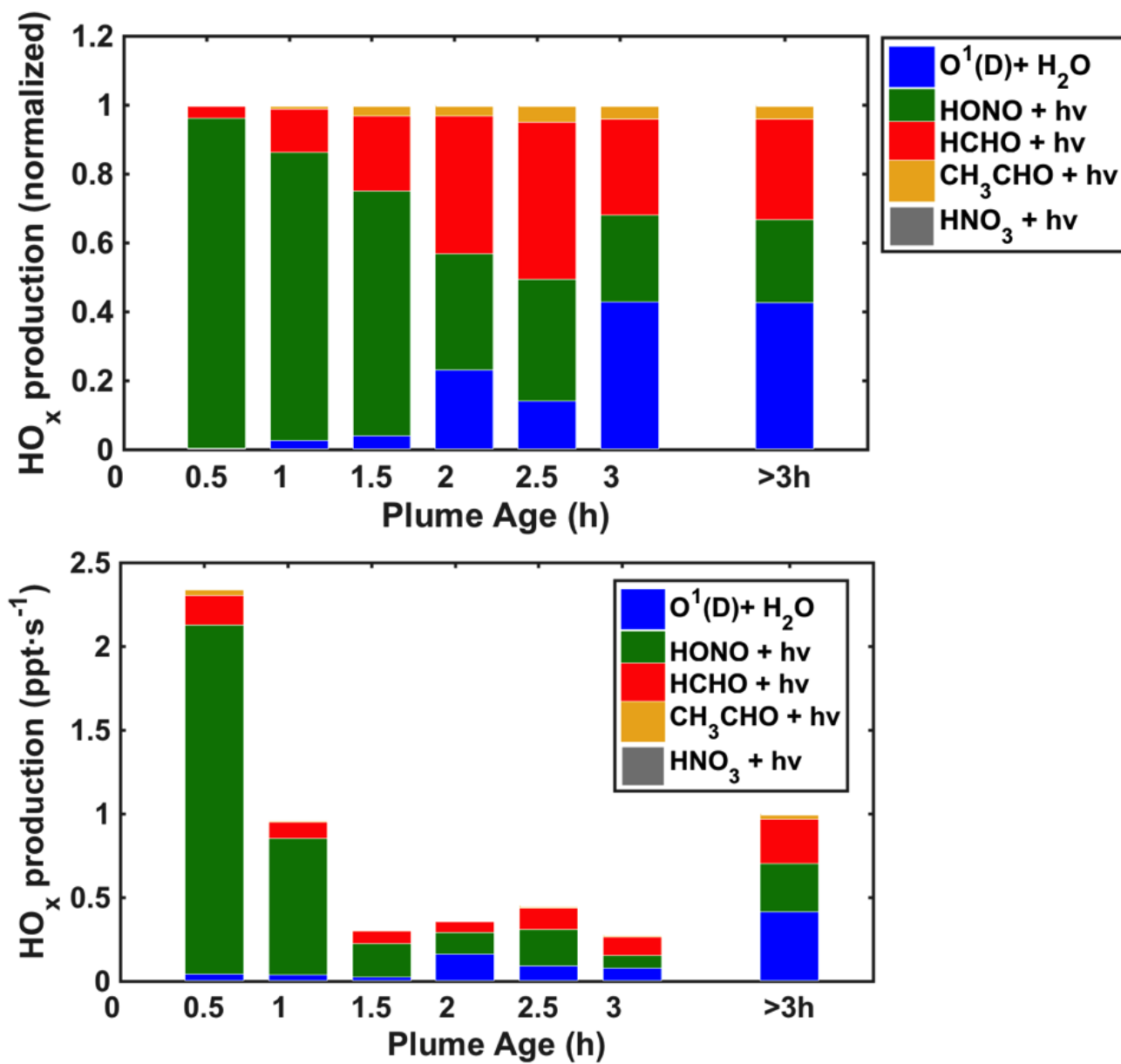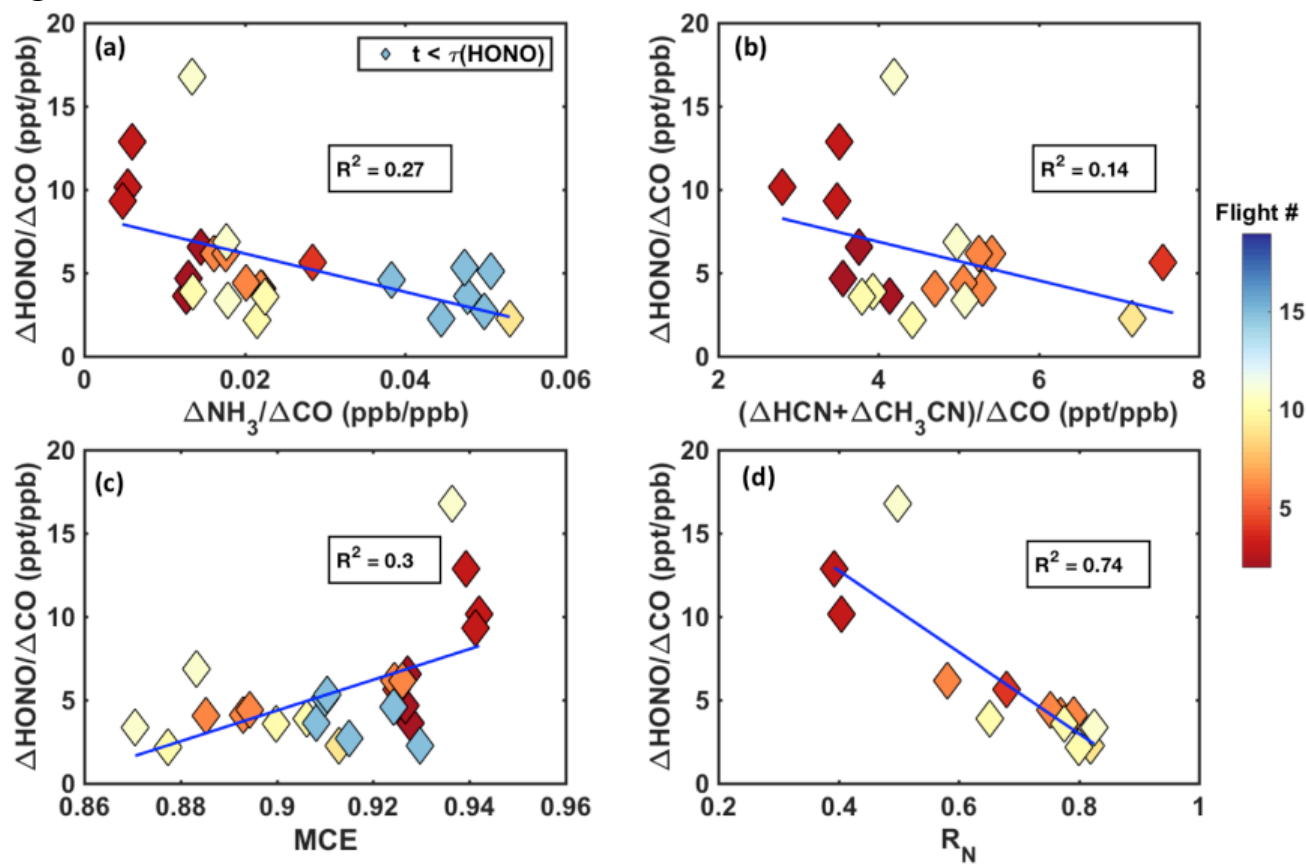
5 **Figure 2**

10

Figure 3

Figure 4

5

5

Figure 5

15
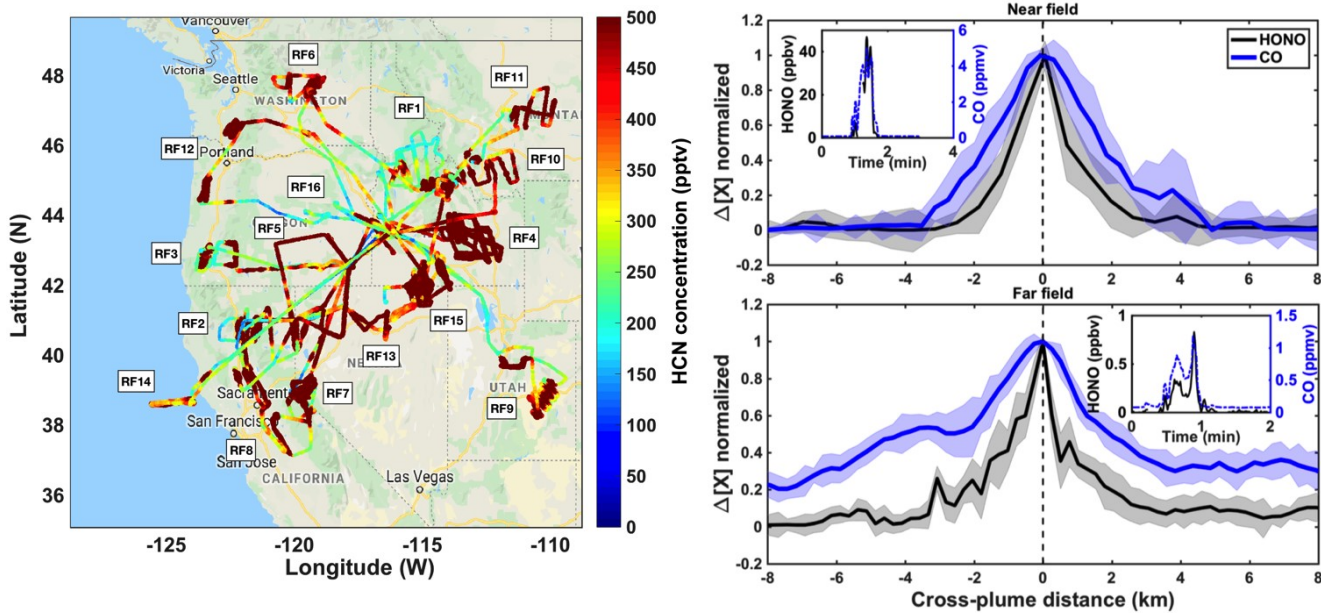
5

References

(1)   Li, Y. Q.; Schwab, J. J.; Demerjian, K. L. Fast Time Response Measurements of Gaseous Nitrous Acid Using a Tunable Diode Laser Absorption Spectrometer: HONO Emission Source from Vehicle Exhausts. *Geophys. Res. Lett.* **2008**, *35* (4). https://doi.org/10.1029/2007GL031218.

(2)   Keene, W. C.; Lobert, J. M.; Crutzen, P. J.; Maben, J. R.; Scharffe, D. H.; Landmann, T.; Hély, C.; Brain, C. Emissions of Major Gaseous and Particulate Species during Experimental Burns of Southern African Biomass. *J. Geophys. Res. Atmos.* **2006**, *111* (4). https://doi.org/10.1029/2005JD006319.

(3)   Elshorbany, Y. F.; Kurtenbach, R.; Wiesen, P.; Lissi, E.; Rubio, M.; Villena, G.; Gramsch, E.; Rickard, A. R.; Pilling, M. J.; Kleffmann, J. Oxidation Capacity of the City Air of Santiago, Chile. *Atmos. Chem. Phys.* **2009**, *9* (6), 2257–2273. https://doi.org/10.5194/acp-9-2257-2009.

(4)   Koppmann, R.; Von Czapiewski, K.; Reid, J. S. *A Review of Biomass Burning Emissions, Part I A Review of Biomass Burning Emissions, Part I: Gaseous Emissions of Carbon Monoxide, Methane, Volatile Organic Compounds, and Nitrogen Containing Compounds A Review of Biomass Burning Emissions, Part I A Review of Biomass Burning Emissions, Part I*; 2005; Vol. 5.

(5)   Chen, L. W. A.; Moosmüller, H.; Arnott, W. P.; Chow, J. C.; Watson, J. G.; Susott, R. A.; Babbitt, R. E.; Wold, C. E.; Lincoln, E. N.; Wei, M. H. Emissions from Laboratory Combustion of Wildland Fuels: Emission Factors and Source Profiles. *Environ. Sci. Technol.* **2007**, *41* (12), 4317–4325. https://doi.org/10.1021/es062364i.

(6)   Veres, P.; Roberts, J. M.; Burling, I. R.; Warneke, C.; De Gouw, J.; Yokelson, R. J. Measurements of Gas-Phase Inorganic and Organic Acids from Biomass Fires by Negative-Ion Proton-Transfer Chemical-Ionization Mass Spectrometry. *J. Geophys. Res. Atmos.* **2010**, *115* (23), D23302. https://doi.org/10.1029/2010JD014033.

(7)   Yokelson, R. J.; Karl, T.; Artaxo, P.; Blake, D. R.; Christian, T. J.; Griffith, D. W. T.; Guenther, A.; Hao, W. M. The Tropical Forest and Fire Emissions Experiment: Overview and Airborne Fire Emission Factor Measurements. *Atmos. Chem. Phys.* **2007**, *7* (19), 5175–5196. https://doi.org/10.5194/acp-7-5175-2007.

(8)   Stockwell, C. E.; Yokelson, R. J.; Kreidenweis, S. M.; Robinson, A. L.; Demott, P. J.; Sullivan, R. C.; Reardon, J.; Ryan, K. C.; Griffith, D. W. T.; Stevens, L. Trace Gas Emissions from Combustion of Peat, Crop Residue, Domestic Biofuels, Grasses, and Other Fuels: Configuration and Fourier Transform Infrared (FTIR) Component of the Fourth Fire Lab at Missoula Experiment (FLAME-4). *Atmos. Chem. Phys* **2014**, *14*, 9727–9754. https://doi.org/10.5194/acp-14-9727-2014.

(9)   Akagi, S. K.; Craven, J. S.; Taylor, J. W.; Mcmeeking, G. R.; Yokelson, R. J.; Burling, I. R.; Urbanski, S. P.; Wold, C. E.; Seinfeld, J. H.; Coe, H.; et al. Evolution of Trace Gases and Particles Emitted by a Chaparral Fire in California. *Atmos. Chem. Phys* **2012**, *12*, 1397–1421. https://doi.org/10.5194/acp-12-1397-2012.

(10)   Stockwell, W. R.; Calvert, J. G. The near Ultraviolet Absorption Spectrum of Gaseous HONO and N2O3. *J. Photochem.* **1978**, *8* (2), 193–203. https://doi.org/10.1016/0047-2670(78)80019-7.

(11)   Barney, W. S.; Wingen, L. M.; Lakin, M. J.; Brauers, T.; Stutz, J.; Finlayson-Pitts, B. J. Infrared Absorption Cross-Section Measurements for Nitrous Acid (HONO) at Room Temperature. *J. Phys. Chem. A* **2000**, *104* (8), 1692–1699. https://doi.org/10.1021/jp9930503.

(12)   Yokelson, R. J.; Christian, T. J.; Karl, T. G.; Guenther, A. The Tropical Forest and Fire Emissions Experiment: Laboratory Fire Measurements and Synthesis of Campaign Data. *Atmos. Chem. Phys.* **2008**, *8* (13), 3509–3527. https://doi.org/10.5194/acp-8-3509-2008.

(13)   Akagi, S. K.; Yokelson, R. J.; Wiedinmyer, C.; Alvarado, M. J.; Reid, J. S.; Karl, T.; Crounse, J. D.; Wennberg, P. O. Atmospheric Chemistry and Physics Emission Factors for Open and Domestic Biomass Burning for Use in Atmospheric Models. *Atmos. Chem. Phys* **2011**, *11*, 4039–4072. https://doi.org/10.5194/acp-11-4039-2011.

(14)   May, A. A.; Lee, T.; Mcmeeking, G. R.; Akagi, S.; Sullivan, A. P.; Urbanski, S.; Yokelson, R. J.; Kreidenweis, S. M. Observations and Analysis of Organic Aerosol Evolution in Some Prescribed Fire Smoke Plumes. **2015**, *15* (11), 6323–6335. https://doi.org/10.5194/acp-15-6323-2015.

(15)   Liu, Z.; Wang, Y.; Gu, D.; Zhao, C.; Huey, L. G.; Stickel, R.; Liao, J.; Shao, M.; Zhu, T.; Zeng, L.; et al. Summertime Photochemistry during CAREBeijing-2007: RO x Budgets and O 3 Formation. *Atmos. Chem. Phys* **2012**, *12*, 7737–7752. https://doi.org/10.5194/acp-12-7737-2012.

(16)   Trentmann, J.; Yokelson, R. J.; Hobbs, P. V.; Winterrath, T.; Christian, T. J.; Andreae, M. O.; Mason, S. A. An Analysis of the Chemical Processes in the Smoke Plume from a Savanna Fire. *Journal of Geophysical Research D: Atmospheres*. June 27, 2005, pp 1–20. https://doi.org/10.1029/2004JD005628.

(17)   Alvarado, M. J.; Prinn, R. G. Formation of Ozone and Growth of Aerosols in Young Smoke Plumes from Biomass Burning: 1. Lagrangian Parcel Studies. *J. Geophys. Res. Atmos.* **2009**, *114* (9), D09306. https://doi.org/10.1029/2008JD011144.

(18)   Alvarado, M. J.; Wang, C.; Prinn, R. G. Formation of Ozone and Growth of Aerosols in Young Smoke Plumes from Biomass Burning: 2. Three-Dimensional Eulerian Studies. **2009**, *114*, D09307. https://doi.org/10.1029/2008JD011186.

(19)   Lee, B. H.; Lopez-Hilfiker, F. D.; Mohr, C.; Kurtén, T.; Worsnop, D. R.; Thornton, J. A. An Iodide-Adduct High-Resolution Time-of-Flight Chemical-Ionization Mass Spectrometer: Application to Atmospheric Inorganic and Organic Compounds. *Environ. Sci. Technol.* **2014**, *48* (11), 6309–6317. https://doi.org/10.1021/es500362a.

(20)   Lee, B. H.; Lopez-Hilfiker, F. D.; Veres, P. R.; McDuffie, E. E.; Fibiger, D. L.; Sparks, T. L.; Ebben, C. J.; Green, J. R.; Schroder, J. C.; Campuzano-Jost, P.; et al. Flight Deployment of a High-Resolution Time-of-Flight Chemical Ionization Mass Spectrometer: Observations of Reactive Halogen and Nitrogen Oxide Species. *J. Geophys. Res. Atmos.* **2018**, *123* (14), 7670–7686. https://doi.org/10.1029/2017JD028082.

(21) Palm, B. B.; Liu, X.; Jimenez, J. L.; Thornton, J. A. Performance of a New Coaxial Ion-Molecule Reaction Region for Low-Pressure Chemical Ionization Mass Spectrometry with Reduced Instrument Wall Interactions. *Atmos. Meas. Tech* **2019**, *12*, 5829–5844. https://doi.org/10.5194/amt-12-5829-2019.

(22) Febo, A.; Perrino, C.; Gherardi, M.; Sparapani, R. *Evaluation of a High-Purity and High-Stability Continuous Generation System for Nitrous Acid*; 1995; Vol. 29.

(23) Xue, Z.; Wu, Z.; Han, S. A Selective Fluorogenic Sensor for Visual Detection of Nitrite. https://doi.org/10.1039/c2ay25107h.

(24) Yokelson, R. J.; Andreae, M. O.; Akagi, S. K. Pitfalls with the Use of Enhancement Ratios or Normalized Excess Mixing Ratios Measured in Plumes to Characterize Pollution Sources and Aging. *Atmos. Meas. Tech.* **2013**, *6* (8), 2155–2158. https://doi.org/10.5194/amt-6-2155-2013.

(25) Briggs, N. L.; Jaffe, D. A.; Gao, H.; Hee, J. R.; Baylon, P. M.; Zhang, Q.; Zhou, S.; Collier, S. C.; Sampson, P. D.; Cary, R. A. Particulate Matter, Ozone, and Nitrogen Species in Aged Wildfire Plumes Observed at the Mount Bachelor Observatory. *Aerosol Air Qual. Res.* **2016**, *16* (12), 3075–3087. https://doi.org/10.4209/aaqr.2016.03.0120.

(26) Karl, T. G.; Christian, T. J.; Yokelson, R. J.; Artaxo, P.; Hao, W. M.; Guenther, A. The Tropical Forest and Fire Emissions Experiment: Method Evaluation of Volatile Organic Compound Emissions Measured by PTR-MS, FTIR, and GC from Tropical Biomass Burning. *Atmos. Chem. Phys.* **2007**, *7* (22), 5883–5897. https://doi.org/10.5194/acp-7-5883-2007.

(27) Garofalo, L. A.; Pothier, M. A.; Levin, E. J. T.; Campos, T.; Kreidenweis, S. M.; Farmer, D. K. Emission and Evolution of Submicron Organic Aerosol in Smoke from Wildfires in the Western United States. *ACS Earth Sp. Chem.* **2019**, *3* (7), 1237–1247. https://doi.org/10.1021/acsearthspacechem.9b00125.

(28) Yokelson, R. J.; Goode, J. G.; Ward, D. E.; Susott, R. A.; Babbitt, R. E.; Wade, D. D.; Bertschi, I.; Griffith, D. W. T.; Hao, W. M. Emissions of Formaldehyde, Acetic Acid, Methanol, and Other Trace Gases from Biomass Fires in North Carolina Measured by Airborne Fourier Transform Infrared Spectroscopy. *J. Geophys. Res. Atmos.* **1999**, *104* (D23), 30109–30125. https://doi.org/10.1029/1999JD900817.

(29) Jaffe, D. A.; Wigder, N.; Downey, N.; Pfister, G.; Boynard, A.; Reid, S. B. Impact of Wildfires on Ozone Exceptional Events in the Western U.S. *Environ. Sci. Technol.* **2013**, *47* (19), 11065–11072. https://doi.org/10.1021/es402164f.

(30) Burling, I. R.; Yokelson, R. J.; Akagi, S. K.; Urbanski, S. P.; Wold, C. E.; Griffith, D. W. T.; Johnson, T. J.; Reardon, J.; Weise, D. R. Airborne and Ground-Based Measurements of the Trace Gases and Particles Emitted by Prescribed Fires in the United States. *Atmos. Chem. Phys.* **2011**, *11* (23), 12197–12216. https://doi.org/10.5194/acp-11-12197-2011.

(31) Müller, M.; Anderson, B. E.; Beyersdorf, A. J.; Crawford, J. H.; Diskin, G. S.; Eichler, P.; Fried, A.; Keutsch, F. N.; Mikoviny, T.; Thornhill, K. L.; et al. In Situ Measurements and Modeling of

Reactive Trace Gases in a Small Biomass Burning Plume. *Atmos. Chem. Phys.* **2016**, *16* (6), 3813–3824. https://doi.org/10.5194/acp-16-3813-2016.

(32)   Koss, A. R.; Sekimoto, K.; Gilman, J. B.; Selimovic, V.; Coggon, M. M.; Zarzana, K. J.; Yuan, B.; Lerner, B. M.; Brown, S. S.; Jimenez, J. L.; et al. Non-Methane Organic Gas Emissions from Biomass Burning: Identification, Quantification, and Emission Factors from PTR-ToF during the FIREX 2016 Laboratory Experiment. *Atmos. Chem. Phys* **2018**, *18*, 3299–3319. https://doi.org/10.5194/acp-18-3299-2018.

(33)   Neuman, J. A.; Trainer, M.; Brown, S. S.; Min, K.-E.; Nowak, J. B.; Parrish, D. D.; Peischl, J.; Pollack, I. B.; Roberts, J. M.; Ryerson, T. B.; et al. HONO Emission and Production Determined from Airborne Measurements over the Southeast U.S. *J. Geophys. Res. Atmos.* **2016**, *121* (15), 9237–9250. https://doi.org/10.1002/2016JD025197.

(34)   Burling, I. R.; Yokelson, R. J.; Griffith, D. W. T.; Johnson, T. J.; Veres, P.; Roberts, J. M.; Warneke, C.; Urbanski, S. P.; Reardon, J.; Weise, D. R.; et al. Laboratory Measurements of Trace Gas Emissions from Biomass Burning of Fuel Types from the Southeastern and Southwestern United States. *Atmos. Chem. Phys* **2010**, *10*, 11115–11130. https://doi.org/10.5194/acp-10-11115-2010.

(35)   Selimovic, V.; Yokelson, R. J.; Warneke, C.; Roberts, J. M.; De Gouw, J.; Reardon, J.; Griffith, D. W. T. Aerosol Optical Properties and Trace Gas Emissions by PAX and OP-FTIR for Laboratory-Simulated Western US Wildfires during FIREX. *Atmos. Chem. Phys* **2018**, *18*, 2929–2948. https://doi.org/10.5194/acp-18-2929-2018.

(36)   Urbanski, S. Wildland Fire Emissions, Carbon, and Climate: Emission Factors. *For. Ecol. Manage.* **2014**, *317*, 51–60. https://doi.org/10.1016/j.foreco.2013.05.045.

(37)   Coggon, M. M.; Veres, P. R.; Yuan, B.; Koss, A.; Warneke, C.; Gilman, J. B.; Lerner, B. M.; Peischl, J.; Aikin, K. C.; Stockwell, C. E.; et al. Emissions of Nitrogen-Containing Organic Compounds from the Burning of Herbaceous and Arboraceous Biomass: Fuel Composition Dependence and the Variability of Commonly Used Nitrile Tracers. *Geophys. Res. Lett.* **2016**, *43* (18), 9903–9912. https://doi.org/10.1002/2016GL070562.

(38)   Ye, C.; Zhou, X.; Pu, D.; Stutz, J.; Festa, J.; Spolaor, M.; Tsai, C.; Cantrell, C.; Mauldin, R. L.; Campos, T.; et al. Rapid Cycling of Reactive Nitrogen in the Marine Boundary Layer. *Nature* **2016**, *532* (7600), 489–491. https://doi.org/10.1038/nature17195.

(39)   Leppälahti, J.; Koljonen, T. Nitrogen Evolution from Coal, Peat and Wood during Gasification: Literature Review. *Fuel Processing Technology*. 1995, pp 1–45. https://doi.org/10.1016/0378-3820(94)00123-B.

(40)   Yokelson, R. J.; Griffith, D. W. T.; Ward, D. E. Open-Path Fourier Transform Infrared Studies of Large-Scale Laboratory Biomass Fires. *J. Geophys. Res. Atmos.* **1996**, *101* (15), 21067–21080. https://doi.org/10.1029/96jd01800.

(41)   Sekimoto, K.; Koss, A. R.; Gilman, J. B.; Selimovic, V.; Coggon, M. M.; Zarzana, K. J.; Yuan, B.; Lerner, B. M.; Brown, S. S.; Warneke, C.; et al. High-and Low-Temperature Pyrolysis

Profiles Describe Volatile Organic Compound Emissions from Western US Wildfire Fuels. *Atmos. Chem. Phys* **2018**, *18*, 9263–9281. https://doi.org/10.5194/acp-18-9263-2018.

(42) Dagaut, P.; Glarborg, P.; Alzueta, M. U. The Oxidation of Hydrogen Cyanide and Related Chemistry. *Progress in Energy and Combustion Science*. February 2008, pp 1–46. https://doi.org/10.1016/j.pecs.2007.02.004.

(43) Ward, D. E.; Radke, L. F. *Emissions Measurements from Vegetation Fires : A Comparative Evaluation of Methods and Results, Fire in the Environment: The Ecological, Atmospheric, and Climatic Importance of Vegetation Fires, Edited By:*; 1993.

(44) Goode, J. G.; Yokelson, R. J.; Susott, R. A.; Ward, D. E. Trace Gas Emissions from Laboratory Biomass Fires Measured by Open-Path Fourier Transform Infrared Spectroscopy: Fires in Grass and Surface Fuels. *J. Geophys. Res. Atmos.* **1999**, *104* (D17), 21237–21245. https://doi.org/10.1029/1999JD900360.

(45) Goode, J. G.; Yokelson, R. J.; Ward, D. E.; Susott, R. A.; Babbitt, R. E.; Davies, M. A.; Hao, W. M. Measurements of Excess O_3, CO_2, CO, CH_4, C_2H_4, C_2H_2, HCN, NO, NH_3, HCOOH, CH_3COOH, HCHO, and CH_3OH in 1997 Alaskan Biomass Burning Plumes by Airborne Fourier Transform Infrared Spectroscopy (AFTIR). *J. Geophys. Res. Atmos.* **2000**, *105* (D17), 22147–22166. https://doi.org/10.1029/2000jd900287.

(46) McMeeking, G. R.; Kreidenweis, S. M.; Baker, S.; Carrico, C. M.; Chow, J. C.; Collett, J. L.; Hao, W. M.; Holden, A. S.; Kirchstetter, T. W.; Malm, W. C.; et al. Emissions of Trace Gases and Aerosols during the Open Combustion of Biomass in the Laboratory. *J. Geophys. Res. Atmos.* **2009**, *114* (19). https://doi.org/10.1029/2009JD011836.

(47) Hansson, K. M.; Samuelsson, J.; Åmand, L. E.; Tullin, C. The Temperature's Influence on the Selectivity between HNCO and HCN from Pyrolysis of 2,5-Diketopiperazine and 2-Pyridone. *Fuel* **2003**, *82* (18), 2163–2172. https://doi.org/10.1016/S0016-2361(03)00206-0.

(48) Hansson, K. M.; Samuelsson, J.; Tullin, C.; Åmand, L. E. Formation of HNCO, HCN, and NH_3 from the Pyrolysis of Bark and Nitrogen-Containing Model Compounds. *Combust. Flame* **2004**, *137* (3), 265–277. https://doi.org/10.1016/j.combustflame.2004.01.005.